Chapter 3

Graphene-Based Metasurface for Tunable Absorption and Transmission Characteristics in the Near Mid-Infrared Region

3.1. Introduction

Electromagnetic (EM) wave absorption concept has been reviewed with its spatial filtering properties in a recent literature termed as 'rasorbers' [264]. Rasorbers have created a great interest among the researchers as well as the defense industry to find suitable applications like sensing, reducing radar cross-section (RCS), satellite-based communication systems, stealth applications, etc. [265]-[268]. Metasurface structures, made out of periodic sub-wavelength unit cells, have been proposed for various frequency-selective applications, including, absorbers, polarization converters, filters, etc. [250], [269]-[271]. Recently, graphene-based metasurfaces have generated potential interest where spectrum tuning can be realized owing to the conductivity modulation of graphene due to the application of impurity doping, external biasing, and mechanical straining [97]-[99]. The terahertz gap is a hotspot for upcoming EM applications towards absorbers, polarization converters, etc. [116]-[117]. It also helps in producing interference-free communication by transmitting the incident EM wave over a chosen band of frequencies beyond the absorption band [272]-[275].

A few metasurface-based three layered rasorbers with metal-dielectric-metal combination were explored in microwave bands [276]-[281], although their fabrications appear quite challenging. Most of them embody lumped circuit elements resulting in an overall bulky configuration. The subsequent developments aiming to terahertz applications used metal-graphene hybrid metasurfaces [282]-[283] to achieve tunability along with reduction in structural thickness.

Those improvements occurred at the cost of reduction in transmission bandwidth. A detailed account of this has been provided later. A pure graphene-based design has been reported in [283] which is structurally simpler compared to the hybrid ones [281]-[282], but at the same time, loses structural compactness as well as effective homogeneity.

The present work addresses the above challenge using much simpler shaped monolayer graphene metasurface with a periodicity reduced by 6 times compared to [283]. The bottom frequency selective surface (FSS) of our proposed structure also bears an innovative shaping on a gold layer which finally results in a noticiable improvement in transmission coefficient up to 0.925 from the earlier reported value 0.72 [283]. A novel scheme for uniform and simultaneous biasing of the graphene metasurface array has been demonstrated for the first time. The full structure has been critically analyzed with the help of exhaustive sets of data obtained using [226].

The design strategy also enhances the EM coupling between the metasurface and FSS layer with enlarged field localization in wave-matter interactions between periodic graphene metasurface and silicon dioxide substrate (SiO_2). This in turn helps in achieving a tunable 10-dB fractional absorption bandwidth up to 70.33%, considerably improved compared to 66.7% reported in [283]. All these improved features are associated with another remarkable characteristic, *i.e.*, its ultrathin configuration ($\lambda_g/10.70$). This indeed can claim to be the thinnest possible rasorber reported so far.

The lack of available experimental setup in our country to fabricate and measure the prototype has been taken care of by confirming the simulated data using an equivalent circuit model. The details of the same have been discussed. The proposed rasorber offers a polarization-independent response along with a tunable absorption band. It promises angular stability for the incident angle up to 40° in case of both TE and TM polarizations of the EM wave.

3.2. Design and Electromagnetic Execution of the Structure

Overall, the structure consists of three different layers composed of top layer square graphene pattern of thickness 1 nm, a 14 µm thick silicon dioxide (SiO_2) block of relative permittivity of 2.3 (tan δ = 0.001) [284]-[285] in the middle and a triangularly-slotted gold metal plate of electrical conductivity (σ) of 4.56×107 S/m at

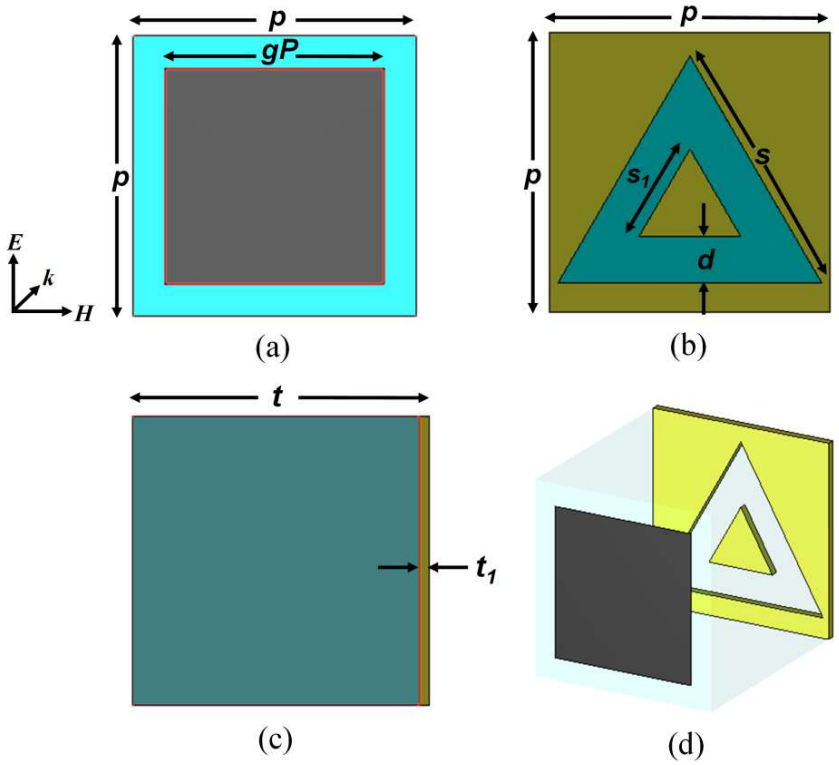

Fig. 3.1. (a) Top view, (b) bottom view, (c) side view and (d) perspective view of the wideband graphene-based metasurface rasorber in the lower MIR region.

the bottom. The top layer is mainly an array of repetitive monolayer graphene pattern of the single element along *xy*-plane perpendicular to the open boundary along the *z*-direction, presented in Fig. 3.1. The open boundary allows the incident EM wave to interact with the overall structure.

The front, back, side and perspective views of the design are explored in Fig. 3.1(a), Fig. 3.1(b), Fig. 3.1(c) and Fig. 3.1(d), respectively. The structural dimensions of the unit cell presented in Fig. 3.1 are finalized after a rigorous parametric study as p = 12 µm, gP = 9 µm, t = 14 µm, d

= 4 µm, s = 11.26 µm and s_1 = 4.33 µm. A single layer CVD grown graphene with 1 nm thickness is the most suitable one for printed absorber technology with all its unique electrical and mechanical properties [287]. All the required properties have been considered while designing a 1 nm thick monolayer graphene geometry in the simulation tool. The interband part of the complex

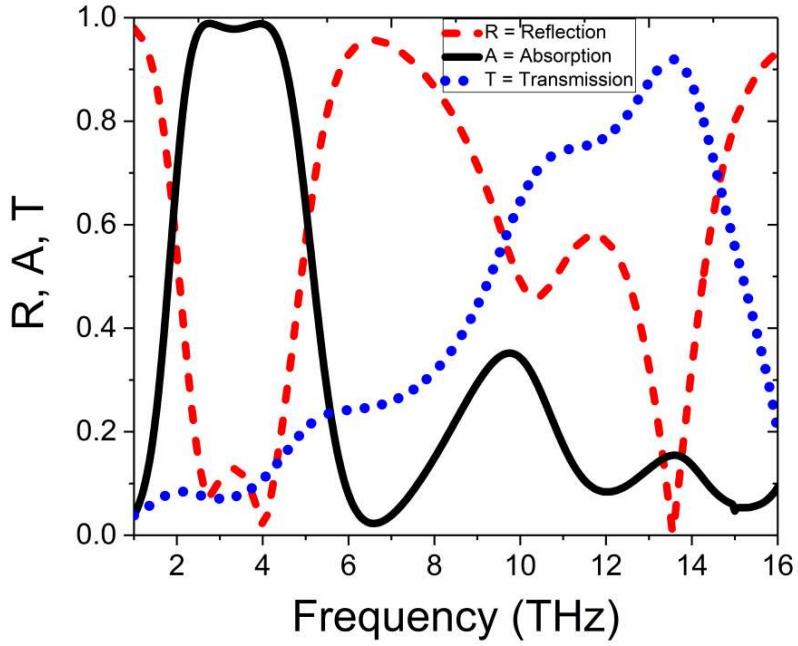

Fig. 3.2. Frequency responses of reflection coefficient (R), transmission coefficient (T) and absorption (A) of EM wave incident on the designed rasorber.

surface conductivity is least effective due to the fact that the Fermi energy (E_f) possesses higher value than 50% of the photon energy validated by Pauli's exclusion principle [18]. The tunable property of graphene due to its conductivity modulation by varying Fermi energy can be monitored externally as given in equations (3.1), (3.2) and (3.3) [288]. In the infrared region, graphene has the surface conductivity formulated by the Drude model. A detailed explanation of the surface conductivity of 2D graphene can be found from the literature [18].

$$E_{\mathrm{f}} = \hbar v_{\mathrm{f}} \sqrt{\frac{\pi \varepsilon_{\mathrm{p}} \varepsilon_o \mu_{\mathrm{c}}}{et^2}} \qquad (3.1)$$

$$\sigma_{\mathrm{g}} = \frac{e^2 E_{\mathrm{f}}}{\pi \hbar^2} \cdot \frac{i}{\omega + i\tau^{-1}} \qquad (3.2)$$

$$\varepsilon(\omega) = 1 + i\frac{\sigma_g(\omega)}{t_g \varepsilon_o(\omega)} \qquad (3.3)$$

Maxwell's equations have been solved for this structure using CST Microwave Studio [226] based on the finite integration technique (FIT) in the frequency domain for calculating reflection, transmission, and absorption characteristics. The thickness of the triangularly slotted bottom layer is higher compared to the skin depth of the gold at the near mid-infrared frequencies. The incident EM wave entered through the top graphene pattern experiences reflections as well as transmission through the whole process. Multiple reflections of the EM wave between the top graphene metasurface and the bottom gold FSS acting as a Fabry-Perot cavity resonance ultimately results in the absorption behavior of the designed prototype. On the contrary, the triangularly-slotted FSS structure on the back generates the transmission band stated earlier. Thus, the structure as a whole, acts as an absorber (2.24 THz-4.67 THz) with a transmission peak at 13.56 THz within the lower terahertz region. The absorptivity has been evaluated from $A = 1 - |R|^2 - |T|^2$, where A = absorptivity, R = reflection co-efficient of the wave incident on the top surface of the design and T = transmission co-efficient of the wave transmitted from the back of the proposed device. The above-said reflection co-efficient, transmission co-efficient, and absorptivity have been shown in Fig. 3.2. It is evident that the reflectivity level is less than 0.5 in the linear scale from 2.24 THz to 4.67 THz deriving an absorption bandwidth of 2.43 THz. The rasorber structure has a transmission peak at 13.56 THz with a fractional bandwidth of 34.01%. The absorptivity is found to be less than 0.2 at the transmission peak of 13.56 THz. The graphene-based rasorber can cover the lower terahertz applications with absorption and transmission characteristics simultaneously in a single module in two different frequency bands. Moreover, this proposed device can achieve tunable characteristics in the absorption band using impurity doping, electrical gating, and mechanical straining of the deposited graphene pattern without changing the physical dimensions of the device. The as-calculated transmission band is found to be stable, and this could be because of

the triangularly-slotted bottom gold layer is independent of the Fermi energy. The array of the top layer square graphene pattern is acting as a conductive sheet of impedance $\mathrm{Z_g} = R + jX$ where R and X are termed as equivalent resistance and reactance of the top layer of the structure proposed in this report. The top metasurface works as an interface between two dielectric media of air and SiO_2, which helps in wave-matter interaction while the EM wave falls onto the proposed geometry. The theory of plane wave propagation through a dielectric medium can be explained by an equivalent transmission line model illustrated in Fig. 3.3 [289]. The characteristic impedance of the free space and silicon dioxide (SiO_2) substrate are denoted as Z_o and Z_h respectively. The effective input impedance of the proposed design is Z_in. The substrate having relative permittivity of ε_h is represented as a transmission line of length h, where h is the thickness of the substrate. The bottom layer bandpass filter can be represented by a parallel combination of inductance-capacitance (L_b & C_b). The complex surface conductivity of graphene is described in some literatures in graphical forms in the lower terahertz region (0.1-10 THz) [290]-[291].

The impedance of the graphene patch can be approximated as given in equation (3.4) where R_graphene and L_graphene can be modulated by varying the chemical potential (μ) of the graphene layer; C is generated due to the mutual coupling between adjacent square shaped graphene patches and is dependent on the background environment and graphene patch geometry [292].

$$Z_\mathrm{patch}(\omega) = R_\mathrm{graphene} + j\omega L_\mathrm{graphene} + \frac{1}{j\omega C} \qquad (3.4)$$

$$R_\mathrm{graphene} = \frac{aP^2}{(P-g)^2} \cdot \mathrm{Re}[\sigma_g]^{-1} \qquad (3.5)$$

$$L_\mathrm{graphene} = \frac{aP^2}{(P-g)^2} \cdot \frac{\mathrm{Im}[\sigma_g]^{-1}}{\omega} \qquad (3.6)$$

$$C = \frac{2P\varepsilon_{eff}}{\pi} \cdot \ln\left[\csc\left\{\frac{\pi g}{2P}\right\}\right] \qquad (3.7)$$

Here, a is the weighted coefficient, $\varepsilon_\mathrm{eff} = \frac{\varepsilon_0(1+\varepsilon_h)}{2}$ is effective permittivity of the mediums

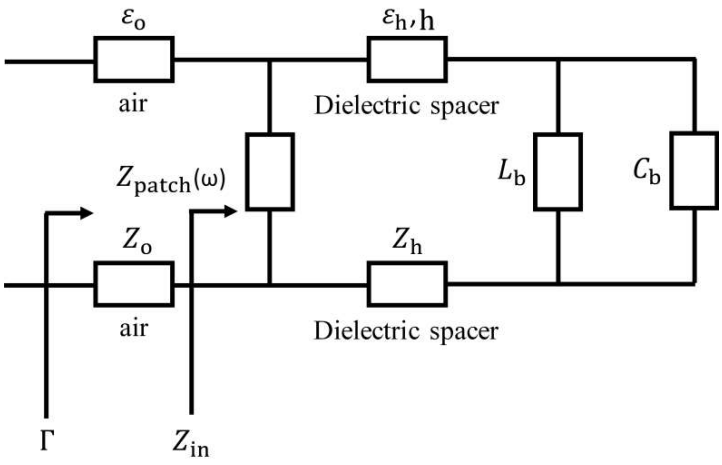

Fig. 3.3. Schematic of the equivalent circuit model for the proposed device.

surrounding the periodic square-shaped graphene patches, ε_0 = permittivity of the free space and ε_h = relative permittivity of the SiO_2 substrate [293]-[295]. The schematic of an equivalent circuit model for the proposed device is provided in Fig. 3. The characteristic impedance of the dielectric spacer of permittivity ε_h can be expressed in equations (3.8) and (3.9) for TE and TM polarizations respectively [296] where θ = incident angle of the EM wave.

$$[Z_h]^{TE} = \frac{\eta_o}{\sqrt{\varepsilon_h - (\sin\theta)^2}} \qquad (3.8)$$

$$[Z_h]^{TM} = \frac{\eta_o\left[\sqrt{\varepsilon_h - (\sin\theta)^2}\right]}{\varepsilon_h} \qquad (3.9)$$

The overall impedance of rest of the circuit along with the dielectric spacer characteristic impedance (Z_h) can thereby be computed by incorporating an open circuit model which is nothing but a bandpass filter produced due to the array of the triangularly cut slots on the bottom gold layer (a parallel circuit combination of L_b , and C_b).

$$[Z_{o.c.}][Z_{s.c.}] = [Z_h]^2 \qquad (3.10)$$

$Z_{s.c.}$ can be computed as shown in equations (3.11) and (3.12) [308].

$$[[Z_h]^{TE}]_{s.c.} = \frac{j\eta_o}{\sqrt{\varepsilon_h - (\sin\theta)^2}} \tan k_{zh}\, h \qquad (3.11)$$

$$[[Z_h]^{TM}]_{s.c.} = \frac{j\eta_o}{\sqrt{\varepsilon_h - (\sin\theta)^2}} \tan k_{zh}\, h \left[1 - \frac{(\sin\theta)^2}{\varepsilon_h}\right] \qquad (3.12)$$

Accordingly, $[[Z_h]^{TE}]_{o.c.}$ and $[[Z_h]^{TM}]_{o.c.}$ can be computed from equation (3.10) by using the respective equations (3.11) and (3.12).

$$[[Z_h]^{TE}]_{o.c.} = \frac{[Z_h]^2}{[[Z_h]^{TE}]_{s.c.}} = \frac{[Z_h]^2}{\frac{j\eta_o}{\sqrt{\varepsilon_h - (\sin\theta)^2}} \tan k_{zh} h} = \frac{[Z_h]^2 \sqrt{\varepsilon_h - (\sin\theta)^2}}{j\eta_o} \cot k_{zh} h \qquad (3.13)$$

$$[[Z_h]^{TM}]_{o.c.} = \frac{[Z_h]^2}{[[Z_h]^{TM}]_{s.c.}} = \frac{[Z_h]^2}{\frac{j\eta_o}{\sqrt{\varepsilon_h - (\sin\theta)^2}} \tan k_{zh} h \left[1 - \frac{(\sin\theta)^2}{\varepsilon_h}\right]} = \frac{[Z_h]^2 \sqrt{\varepsilon_h - (\sin\theta)^2}}{j\eta_o} \cot k_{zh} h \left[1 - \frac{(\sin\theta)^2}{\varepsilon_h}\right] \qquad (3.14)$$

Hence, the overall input impedance (Z_{in}) can be calculated as a parallel combination of $Z_{patch}(\omega)$ and $[Z_h]_{o.c.}$ as provided in equation (3.15).

$$Z_{in} = Z_{patch}(\omega) || [Z_h]_{o.c.} \qquad (3.15)$$

The reflection coefficient (R) can be calculated employing equation (3.16).

$$R = \frac{Z_{in} - [Z_h]_{o.c.}}{Z_{in} + [Z_h]_{o.c.}} \qquad (3.16)$$

The transmission coefficient (T) can also be calculated from the calculated impedance in equation (3.16) by using concept stated in [297].

3.3. Validation of the Simulated Results

The EM simulated results have been validated with the help of a circuit model approach. The circuit representation has been performed using Keysight ADS tool [298] for the proposed graphene-based rasorber to validate its performance further as verified from Fig. 3.4. First, the circuit model of the periodically arranged square graphene patch-based absorber has been carried out by taking the bottom surface with complete gold metallic plate. A square graphene patch can be modeled as a series combination of a resistance, an inductance and a capacitance (R, L_2 and C_2). The dual nature of inductive-capacitive effect [293] has been taken care of by using the circuit components L_1 and C_1 under the influence of the periodic graphene patches as

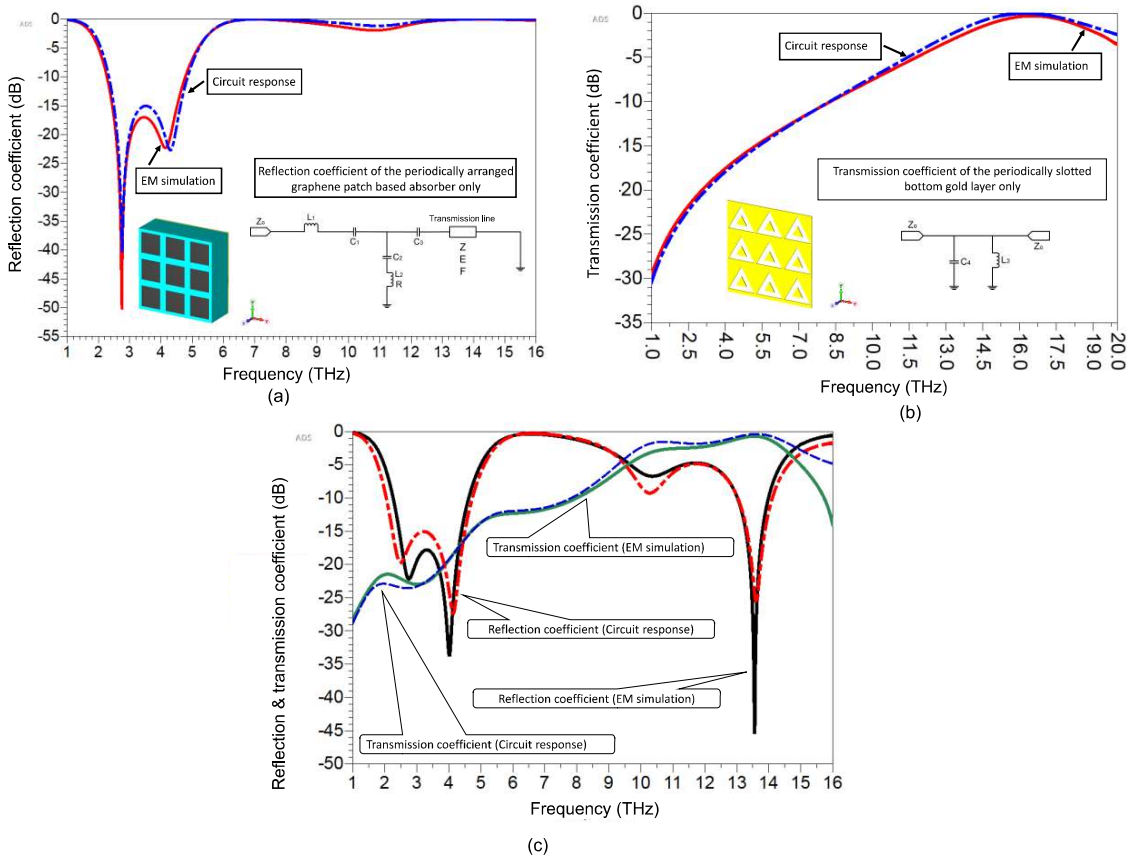

Fig. 3.4. Spectral responses of (a) reflection characteristic of the periodic square graphene patch-based absorber only, (b) transmission characteristic of the periodically-slotted bottom gold layer only, and (c) comparison of both reflection and transmission responses between EM-simulation and equivalent circuit modeling of the proposed graphene based rasorber.

shown in the inset of Fig. 3.4(a). A transmission line has been considered as an equivalent circuit component for the silicon dioxide (SiO_2) substrate as it (SiO_2 substrate) can modify the phase of the EM wave. The corresponding response of the reflection coefficient and the circuit model have been presented in Fig. 3.4(a) where it has been compared with the numerically simulated performance. It has been observed that the responses are in good agreement. The lumped circuit component values for Fig. 3.4(a) are given as: $C_1 = 0.505$ pF, $C_2 = 0.1158$ fF, $C_3 = 169.9802$ fF, $L_1 = 5\times 10^{-5}$ nH, $L_2 = 19.1315$ pH, R = 272.327 Ω, Z = 223.686 Ω., E = 214° and F = 8.5 THz, where Z, E and F signify the characteristics impedance, phase and frequency of operation of the transmission line.

The circuit modeling of the bottom gold FSS layer containing an array of triangular slots has

also been performed separately as depicted in Fig. 3.4(b). The triangularly-slotted bottom gold layer can be implemented as a parallel combination of capacitance (C_4) and inductance (L_3) (identical to L_b and C_b discussed earlier in the theoretical modeling) to produce the bandpass filtering response at the desired band. The circuit component values for Fig. 3.4(b) are provided as: C_4 = 0.107105 fF and L_3 = 0.898078 pH. Thereafter, both the circuits have been combined together to realize the complete rasorber device with identical reflection and transmission

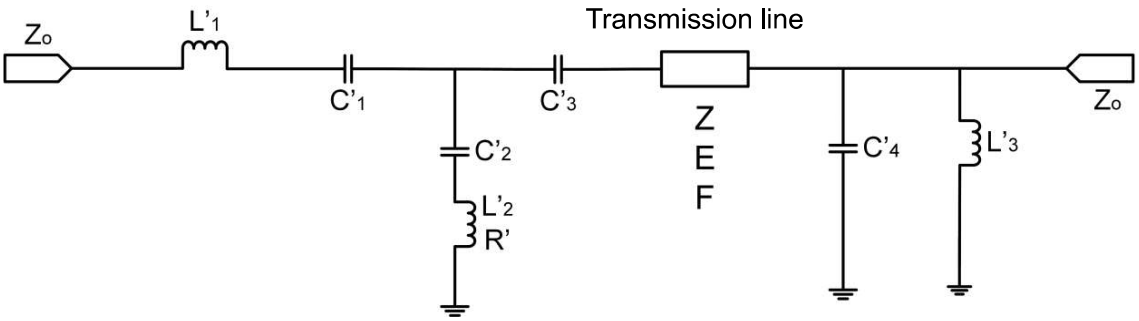

Fig. 3.5. Equivalent circuit model for the proposed graphene based rasorber.

characteristics produced from the EM simulation of the same, as shown in Fig. 3.4(c). The corresponding circuit model has been presented in Fig. 3.5. The optimized circuit component values for Fig. 3.5 are provided in Table 3.1.

Table 3.1. RLC Circuit Component Values for the Proposed Rasorber

RLC Components	Derived Component Values
C'_1	99.9025 pF
C'_2	0.18 fF
C'_3	199.9736 fF
C'_4	0.175 fF
L'_1	5×10^{-5} nH
L'_2	14.0375 pH
L'_3	0.899239 pH
R'	272.74 Ω
Z	223.686 Ω
E	214°
F	8.5 THz

EM wave absorbed in the lower terahertz region is possessing a wide bandwidth as well as transmitted through the structure at a higher terahertz band. In the absorption band, the top graphene pattern acts as a matching circuit between air and SiO_2. We found that in the transmission band, the periodically-arranged triangularly-slotted bottom metal plate is working as an FSS bandpass filter, as shown in Fig. 3.4(b). When the incident EM wave enters into the SiO_2 substrate, the attenuation process is generally dependent on the electrical permittivity and magnetic permeability of the propagating medium (here SiO_2). Overall, the energy of the incident EM wave is being reduced, which is caused due to the destructive wave interference realized through multiple reflections of the EM wave between the top layer and bottom layer as validated by Fabry Perot cavity resonance [26].

The leaky-wave theory concept is also applicable to the layered structures consisting of two periodically-slotted metal surfaces printed on the two opposite sides of a substrate and other configurations [299]. The enhanced transmission has been achieved owing to the excitation of a leaky mode. The periodically-slotted pattern on the bottom surface of the proposed device enables the normally bound (non-leaky) surface plasmon mode converted into a leaky plasmon one. The dimension of the periodic structures is chosen in such a way that the leaky mode radiates at broadside, providing an enhanced directional field and thereby an enhanced transmission has been achieved in the terahertz region [300]. When surface plasmon resonance takes place on a smooth surface, standing wave is generated and the periodicity is chosen as per the condition mentioned in equation (3.17) provided β^{p} is the phase constant of the surface plasmon mode on the smooth surface and P is the associated periodicity of the structure.

$$\beta^{\mathrm{p}} P = 2\pi \qquad (3.17)$$

In case of leaky surface plasmon mode, equation (3.17) is modified as equation (3.18) where β^{LM} is the phase constant of the leaky plasmon mode on the periodic surface.

$$\beta^{\mathrm{LM}} P = 2\pi \qquad (3.18)$$

The leaky mode pattern can be derived from the complex wavenumber of the leaky plasmon mode by incorporating the wave number to approximate the amplitudes of current on the periodically-slotted metal layer on the backside of the proposed device as given by equation (3.19) where k_{LM} is the wavenumber corresponding to the leaky plasmon mode and α_{LM} is the attenuation constant of the leaky plasmon mode on the periodic surface.

$$k_{\mathrm{LM}} = \beta^{\mathrm{LM}} - j\alpha^{\mathrm{LM}} \qquad (3.19)$$

The phase constant (β) and attenuation constant (α) can be calculated from the reflection coefficient and reflection phase of the periodic surfaces employing the dispersion relationship [301]-[303]. Fabry perot-leaky wave antenna concept (FP-LWA) based on graphene has been elaborately discussed in [304].

3.4. Simulated Outputs and Explanations

The dimension of the square-graphene patch arm was estimated in such a way that the coupling between the neighbouring graphene patterns would be maximum with the enhancement of the wave-matter interaction. At the same time, the thickness of SiO_2 is determined in a way that the coupling between the top layer and the bottom layer becomes maximum within the absorption band. After that, the dimensions of the triangularly slotted FSS are finalized to achieve the transmission band characteristics.

The parametric study starts with the variation of graphene patch size (*gP*) where an effective wave-matter interaction takes place when *gP* = 9 μm on the SiO_2 substrate and is demonstrated in Fig. 3.6. The spanning of the graphene layer on the SiO_2 substrate varies while altering *gP*; thereby modifying wave-matter interaction for every value of *gP*, producing different absorption responses. The transmission curve is stable in nature as no structural change has been applied to the triangularly-slotted bottom gold surface. The variation in substrate thickness tailors the coupling strength between the top layer and bottom layer. Correspondingly, the absorption and transmission characteristics have also been varied. The

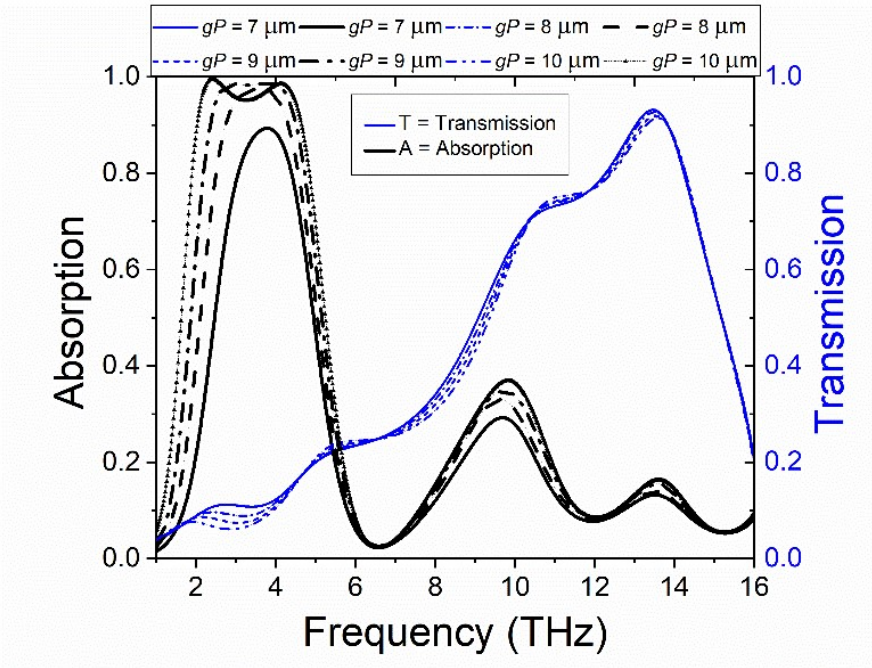

Fig. 3.6. Absorption and transmission behavior of the proposed design with the variation of graphene patch dimensions (*gP*).

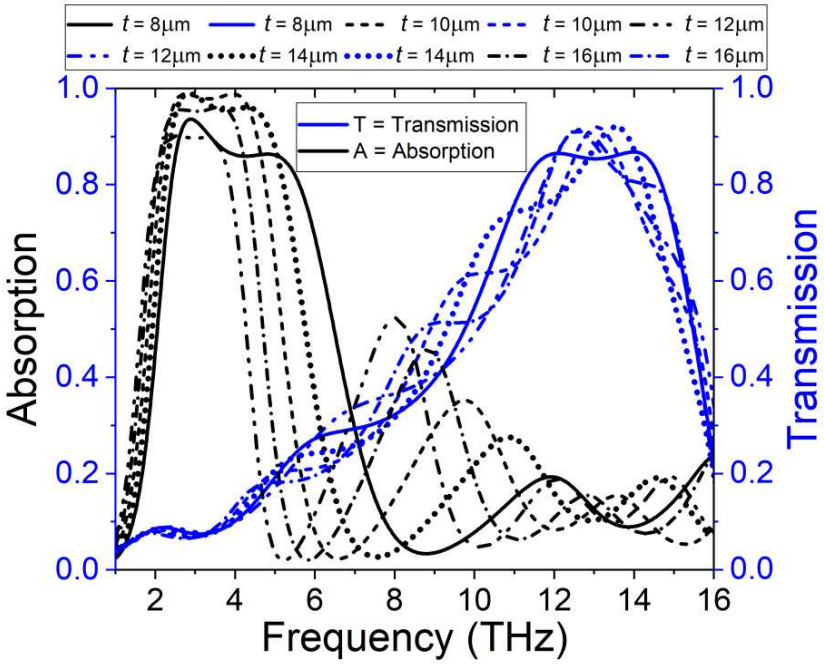

Fig. 3.7. Absorption and transmission behavior of the proposed design with the variation of substrate thickness (*t*).

highest absorptivity peak with the widest bandwidth and the highest transmission peak was achieved when t = 14 μm, as shown in Fig. 3.7. Graphene exhibits more metallic-type conductivity than semiconductor type with the increase of E_f [105].

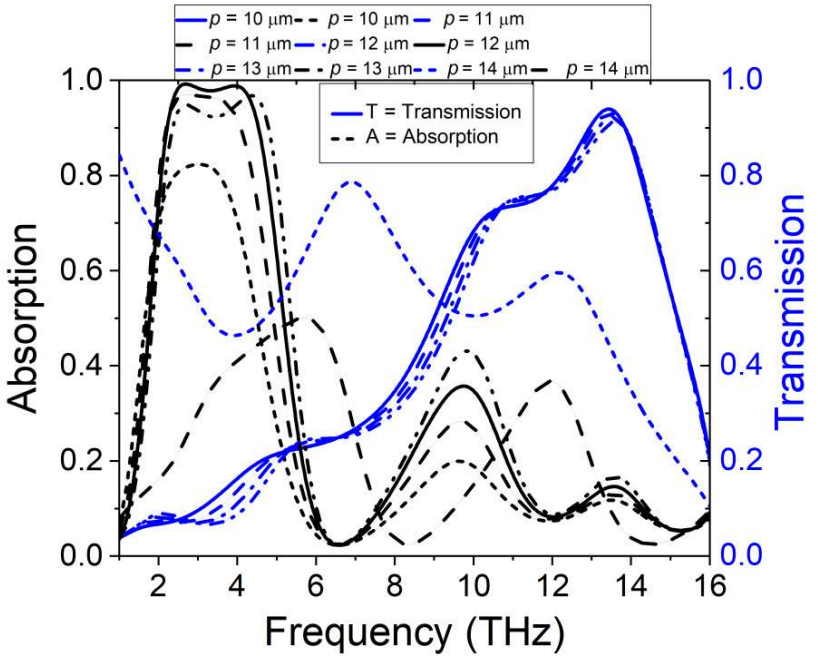

Fig. 3.8. Absorption and transmission behavior of the proposed design with the periodicity (p) variation.

The response of the structure was studied under the variation of the periodicity (p) of the unit cell. Periodicity determines the overall compactness of the structure. It also provides a measure of effective inductance and capacitance among the unit cells; thereby providing resonance. One

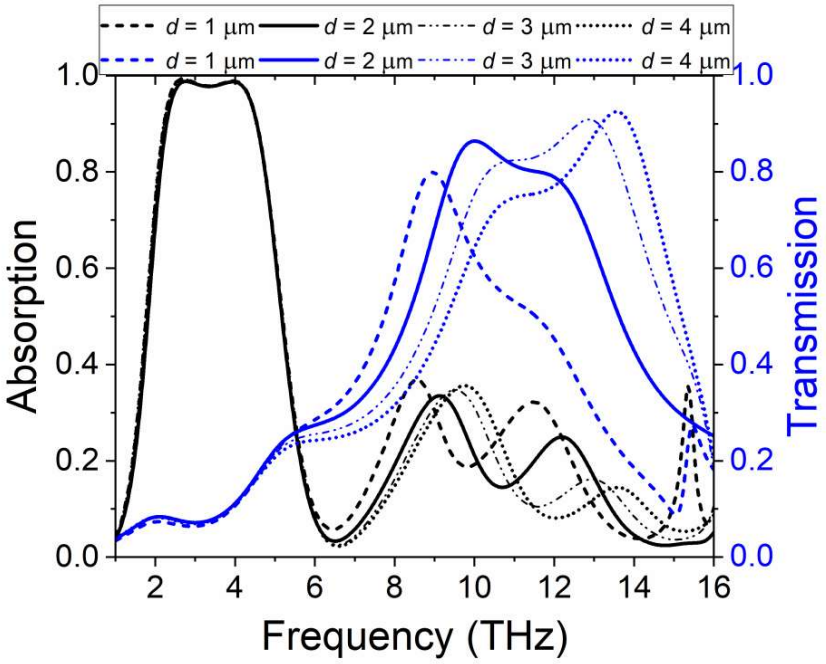

Fig. 3.9. Absorption and transmission behavior of the proposed design with the triangular slot-gap (d) variation.

can find from Fig. 3.8 that the absorption band has been undergoing massive changes, while periodicity variation unlikely changes the transmission band.

The triangular slot size of the back-metal structure has been shaped up by changing the width of the slot as well as the position of the slot. The above change is made by making variations in "*d*" defined in Fig. 1. The corresponding variations in absorption and transmission characteristics have been incorporated in Fig. 3.9. It has been observed from Fig. 3.9 that the variation in *d* does not contribute to any change in the absorption band while the response in the transmission band gets altered. The conductivity of graphene can be modulated by impurity doping or external electrical biasing or mechanical straining [97]-[99]. Relaxation time (τ) is termed as the time duration between two consecutive collisions of the electrons, and it is varied to check the absorption and transmission behavior of the rasorber [305]. Less collision of electrons will add more electrical conductivity in the graphene layer. Relaxation time (τ) is inversely proportional to

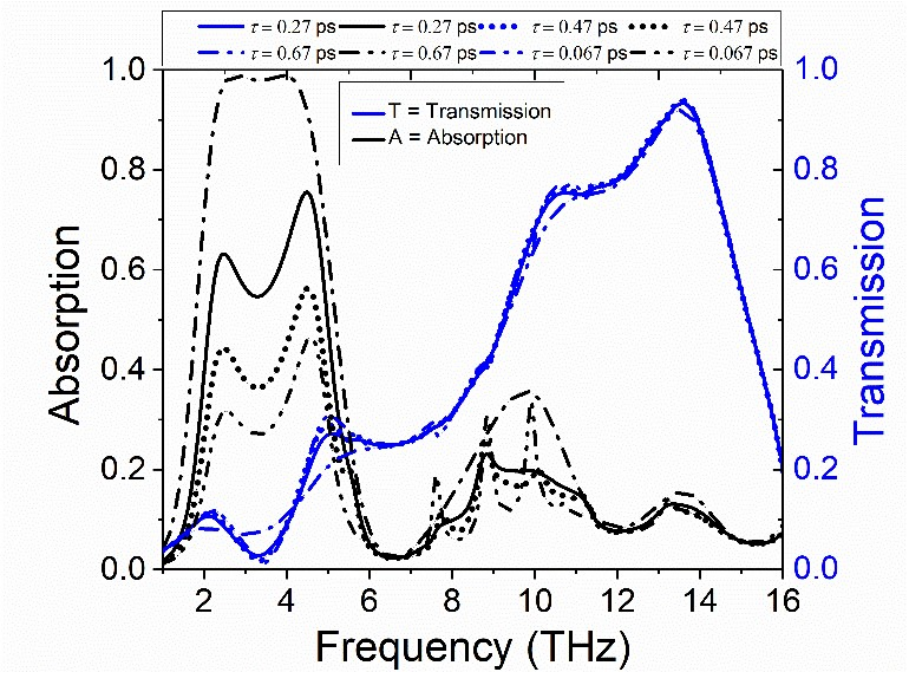

Fig. 3.10. Responses of the wide absorption bandwidths under different values of relaxation time (τ).

the plasmon propagation distance. The best performance is achieved at τ = 0.06 ps as shown in Fig. 3.10, and in this case, the plasmon propagation distance is maximum; thereby the conductivity of the top graphene pattern is maximum, which results in the maximum absorptivity of the proposed device.

During the fabrication of graphene using CVD, proper precautions should be taken to maintain the optimized film quality [306]. Two types of losses occur in this type of proposed device during biasing of the same, *viz.*, graphene ohmic loss and graphene plasmonic loss. For biased graphene, its chemical potential μ has been explored both theoretically [307]-[308] and experimentally [309] to vary over the range from 0 to 1 eV. The relaxation time (τ) varies from 0 to 3 ps in the lower THz domain [310]. The above said two facts are maintained while designing the proposed nano device. In this condition, the graphene layer acts as a good conductor with a nonnegligible ohmic losses [311]-[312]. The second one is plasmonic loss on the graphene surface attributing due to the surface plasmon polariton (SPP). The plasmonic loss is expressed by dissipation loss (α_{SPP}) by the equation expressed in (3.20) where $\phi_0 = \left(\frac{1}{2}\right)\arctan\left(\frac{\pi}{\Delta}\right)$, $\pi = -2\sigma_R\sigma_J$ and $\Delta = [\sigma_R]^2 - [\sigma_J]^2 - \frac{4}{{\eta_o}^2}$. η_o is the characteristic impedance of the vacuum, σ_R is the resistive conductivity of graphene surface, σ_J is the reactive surface conductivity of graphene surface. The surface conductivity of graphene (σ) is strongly dependent on μ and τ values due to which minimum plasmonic loss takes place [312]-[313].

$$\alpha_{SPP} = -\frac{\sqrt[4]{\Delta^2+\pi^2}}{[\sigma_R]^2+[\sigma_J]^2}\left[\sigma_J\cos\phi_0 + \sigma_R\sin\phi_0\right] \qquad [3.20]$$

This chemical potential (μ) is again a function of its Fermi energy and hence the applied DC bias across it. An improved biasing scheme relative to the earlier approaches [281]-[283] has been introduced in our design which is practically viable. This adds an extremely thin ion gel layer (200 nm) with nondispersive permittivity 1.82 on top of the graphene surface as clearly indicated in Fig. 3.11(a). Such idea has been adopted here from the transistor layout of [314]-

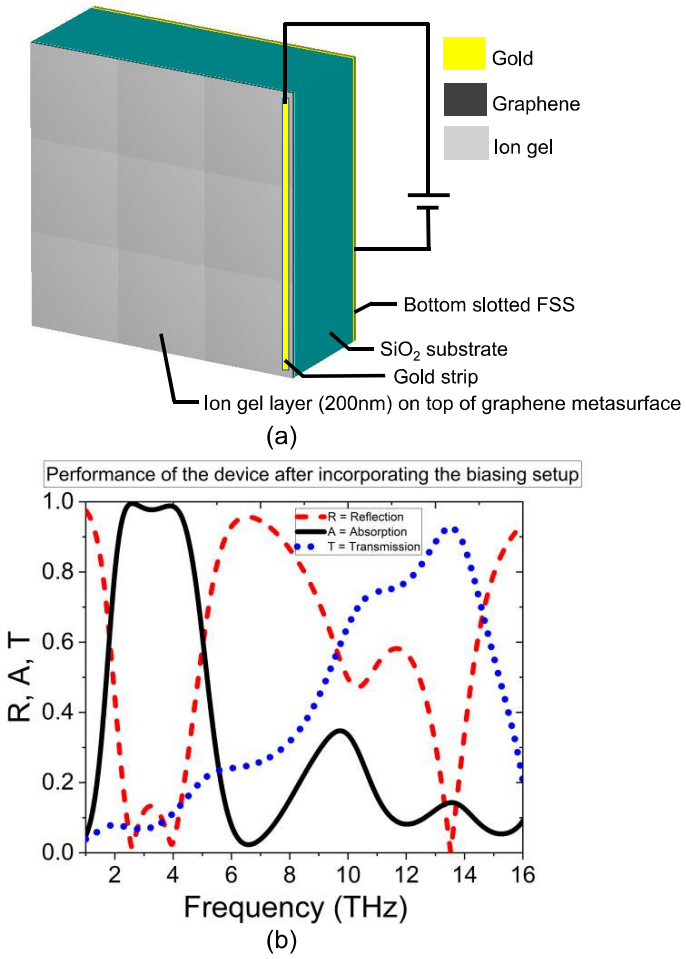

Fig. 3.11. (a) Biasing set-up for the proposed rasorber and (b) frequency responses of reflection (R), absorption (A) and transmission (T) coefficients of the designed rasorber while considering biasing scheme.

[317] and implemented here for the first time for simultaneous and uniform biasing of each unit of the graphene metasurface. The periodically arranged graphene patches are not connected to each other. So, the ion-gel layer has been introduced in the design. Ion-gel is one of the most efficient dielectrics for realizing broadly tunable graphene plasmons with least change in voltage modulation [317]. This type of configuration produces a long-term modulation state due to the low mobility of the ions in the ion-gel layer to form an electric double layer at the graphene-ion-gel interface [317]. An ultrathin gold strip is strategically connected to a border line of ion gel which provides the DC connectivity for the biasing purpose. This is claimed as a novel aspect of realizing an actively tunable graphene

metasurface-based rasorber. The reflection (R), absorption (A) and transmission (T) coefficients responses of the designed rasorber have been studied further while considering the biasing scheme illustrated in Fig. 3.11(a). The corresponding responses have been presented in Fig. 3.11(b). A negligible shift has been experienced along the spectral axis of reflection (R), absorption (A) and transmission (T) coefficients responses as compared to Fig. 3.2 due to the thin superstrate cover of the ion gel layer. It can be observed that without the ion gel superstrate cover the proposed device achieves 90% absorptivity bandwidth of 2.32 THz in between 2.22 THz and 4.54 THz while the implementation of ion gel superstrate cover on the same device yields 90% absorptivity bandwidth of 2.36 THz between 2.14 THz and 4.50 THz.

Its absorption and transmission characteristics as functions of μ values are examined in Fig. 3.12(a), blown up in Fig. 3.12(b) and (c) for clear understanding. It promises a wide range of absorptivity from 60% (μ = 0.3 eV) to 99.9% (μ = 1 eV) which was not revealed in the earlier demonstrations e.g., [281]-[283]. In addition, a new useful feature has been documented in our results: the EM response becomes tunable in the spectral domain e.g., between 1 THz and 1.5 THz (μ = 0.3 eV) and also between 4.4 THz and 6.3 THz (μ = 1 eV). The transmission response (T) around 13.56 THz remains nearly unaltered. The reason is its gold-based FSS layer which is non-responsive to μ variation and thereby causing null effect. The proposed device has been designed with multiple periodically slotted bottom gold layers (PSBGLs) to check the enhanced transmission response of the device. The pictorial representations of the multiple PSBGLs are illustrated in Fig. 3.13 (a, b, c, & d) and the corresponding transmission responses are shown in Fig. 3.14. The transmission response is widely spanned and slightly overlapped with the absorption response, as confirmed from Fig. 3.2. The increasing number of PSBGLs leads to sharp and wideband transmission response including the proposed transmission frequency band at 13.56 THz, as shown in Fig. 3.14. The reason behind this fact is that the

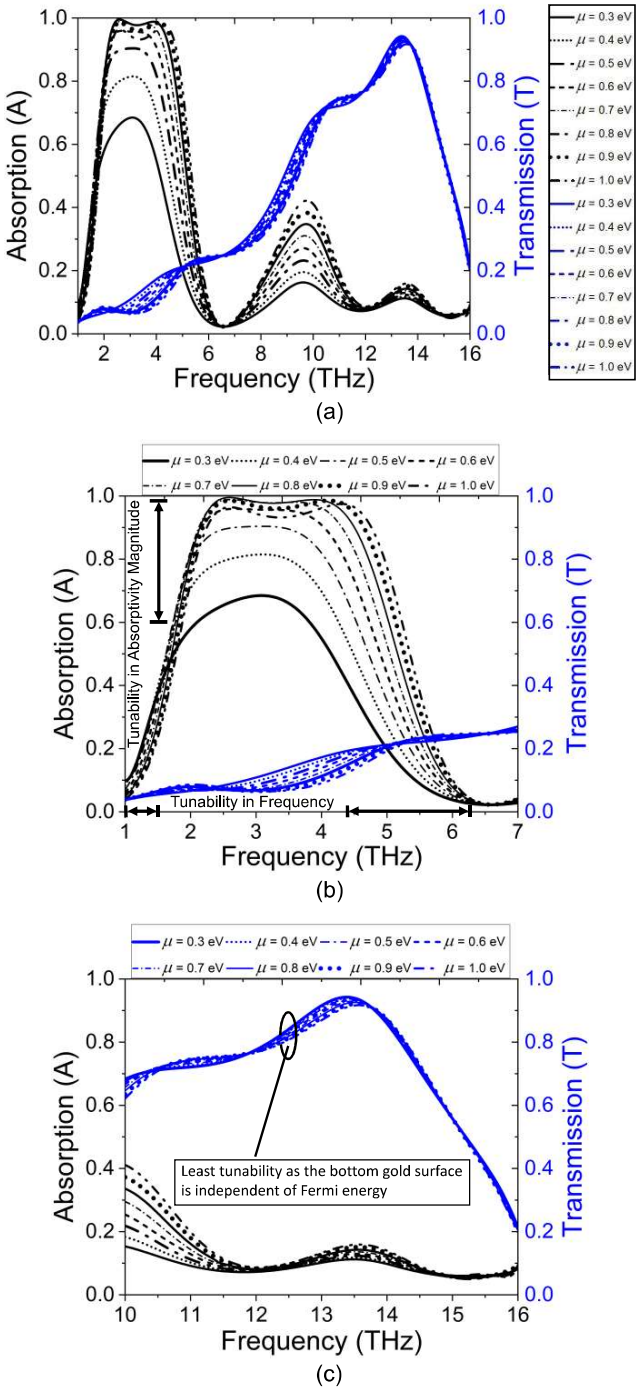

Fig. 3.12. (a). The absorption and transmission behavior of the proposed device under variable DC biasing and blown up in Fig. 12(b) and (c) for clear understanding.

increasing number of PSBGLs increases the order of the bandpass filtering response around the transmission band [318]-[319]. The air gap between the PSBGLs can be realized using polystyrene foam compatible for terahertz frequencies [320]. Therefore, one can conclude that

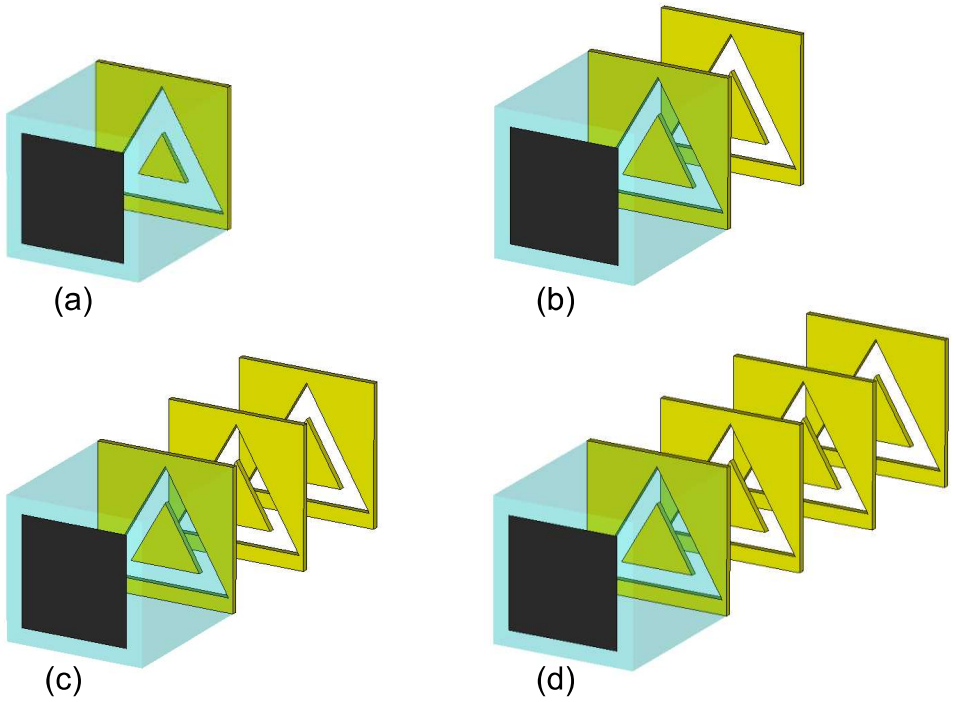

Fig. 3.13. Different configurations of the proposed device with (a) one PSBGL, (b) two PSBGLs, (c) three PSBGLs, and (d) four PSBGLs.

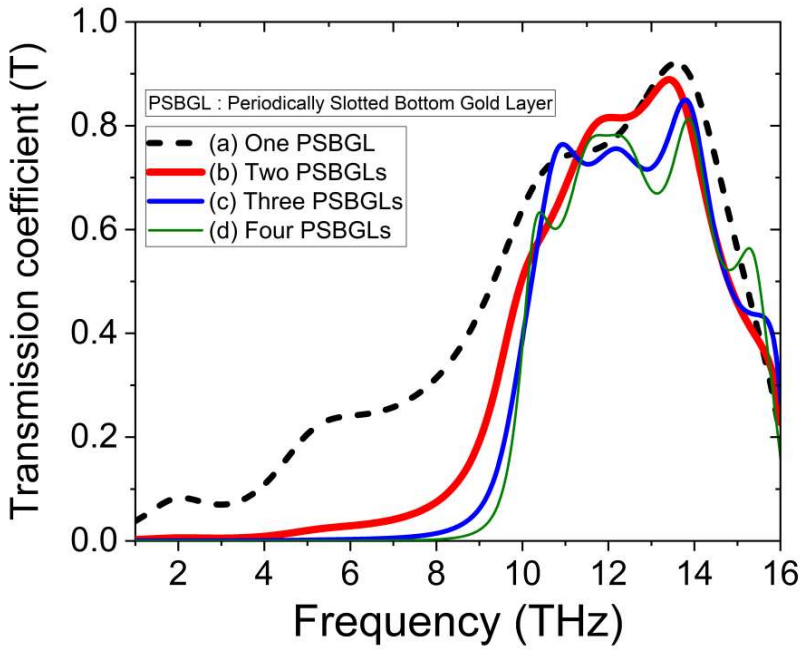

Fig. 3.14. Transmission responses (T) of the proposed device under different configurations of the periodically slotted bottom gold layer (PSBGL).

the transmission response of the terahertz rasorber devices can be improved using multiple layers of the periodically-arranged triangularly-slotted bottom gold layer. The gap between the PSBGLs is set to 13 μm for the optimized transmission performance of the device. Thus, a trade-off between thickness and transmission response of the proposed device can be achieved. It can be concluded from Fig. 3.15 and Fig. 3.16 that the designed prototype provides the almost polarization-independent spectral response of absorption and transmission band under different polarization angles (ϕ) for both TE and TM modes. The behavior of the proposed rasorber is

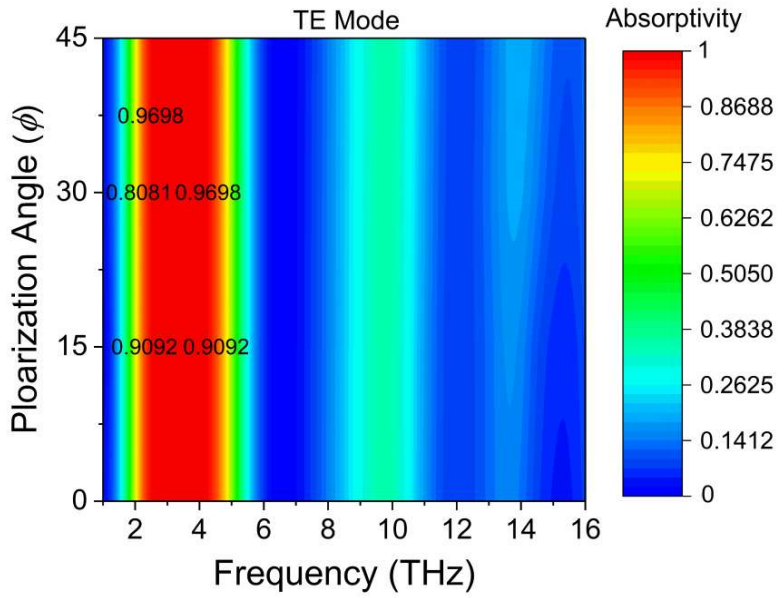

Fig. 3.15 Response of the proposed rasorber as a function of polarization angles (ϕ) and frequency (THz) in TE polarization.

represented together as a function of the polarization angle (ϕ) and frequency (THz). The variations in absorption are constant due to the four-fold symmetry of the top graphene layer. The variations in the transmission characteristics are in a negligible shifted form because of the two-fold symmetry of the designed triangular slot on the bottom layer. The rasorber also needs to be angularly stable, *i.e.*, whether it can perform efficiently under the different angle of incidence (θ) of the EM wave. Therefore, the performances of the structure have been checked under oblique incidence of EM wave. The proposed graphene-based rasorber exhibits stable

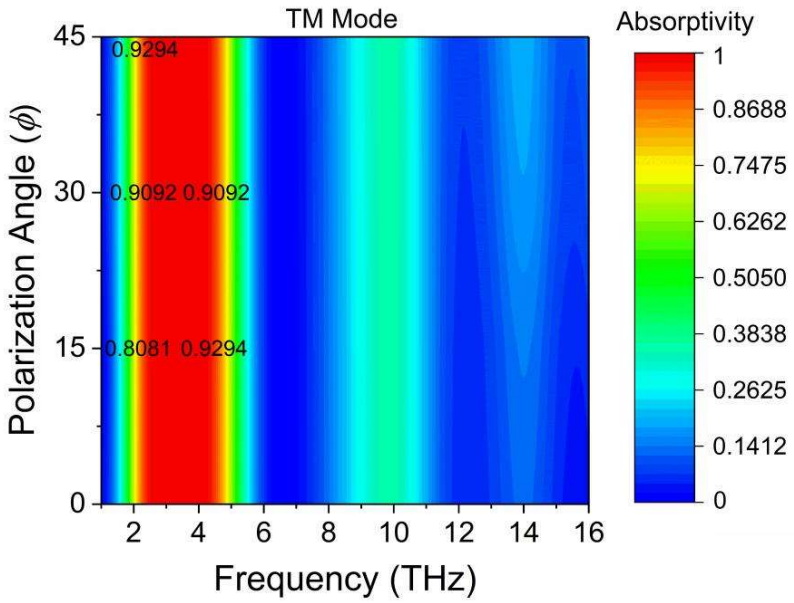

Fig. 3.16. Response of the proposed rasorber as a function of polarization angles (ϕ) and frequency (THz) in TM polarization.

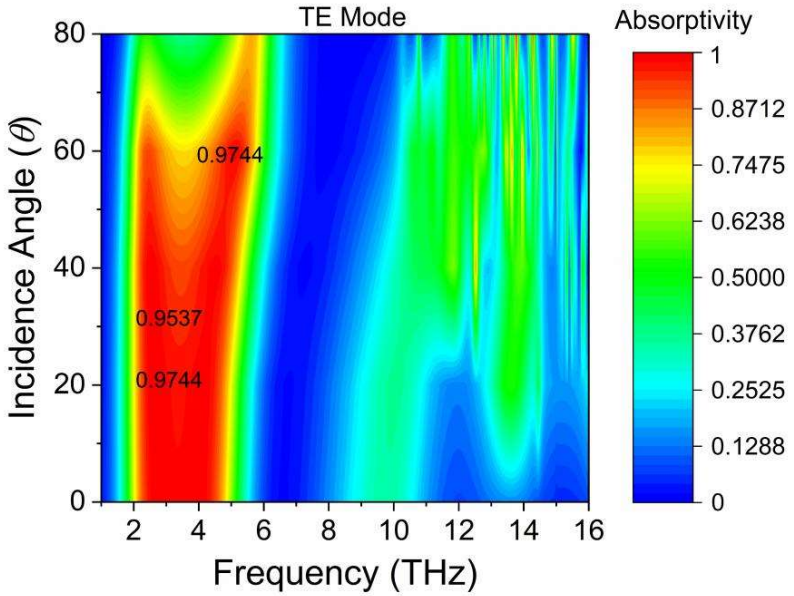

Fig. 3.17. Response of the proposed rasorber as a function of different incident angles (θ) and frequency (THz) in TE polarization.

performances in terms of absorption characteristics up to θ = 40° for both TE and TM polarizations as shown in Fig. 3.17 and Fig. 3.18, respectively. The rasorber also provides good performance with negligible insertion loss in the passband under the normal incidence of the electromagnetic wave as can be verified from Fig. 3.17 and Fig. 3.18. The insertion loss in the

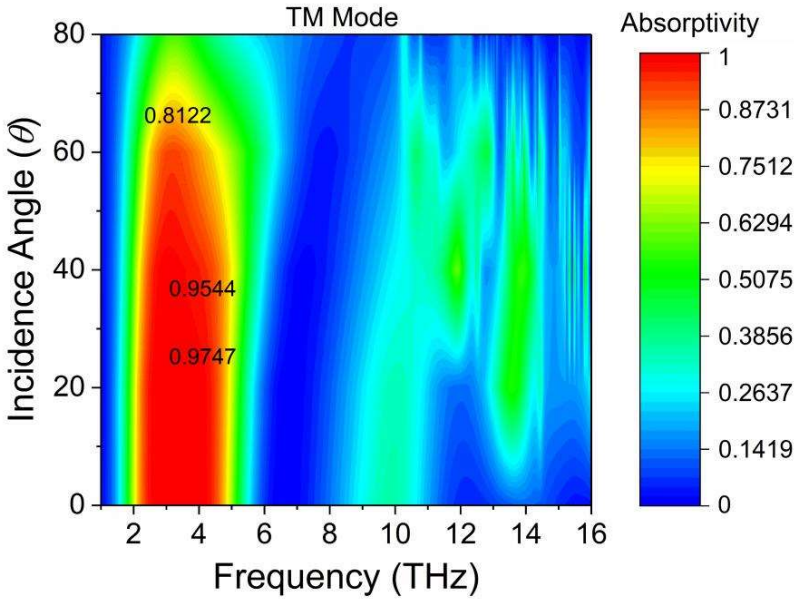

Fig. 3.18. Response of the proposed rasorber as a function of different incident angles (θ) and frequency (THz) in TM polarization.

pass band can be neglected as it is very less under TM polarization of EM wave as verified from Fig. 3.18. An increasing nature of the insertion loss in the passband has been experienced in Fig. 3.17.

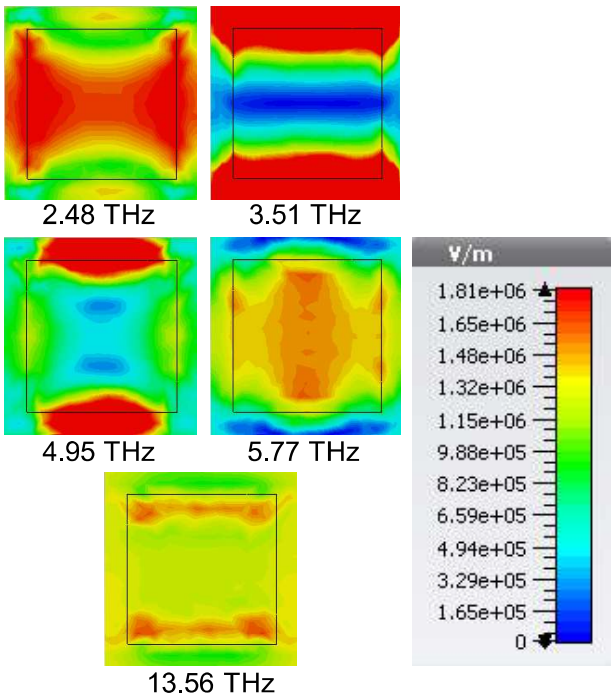

Fig. 3.19. Electric field distributions of the overall structure at different frequencies.

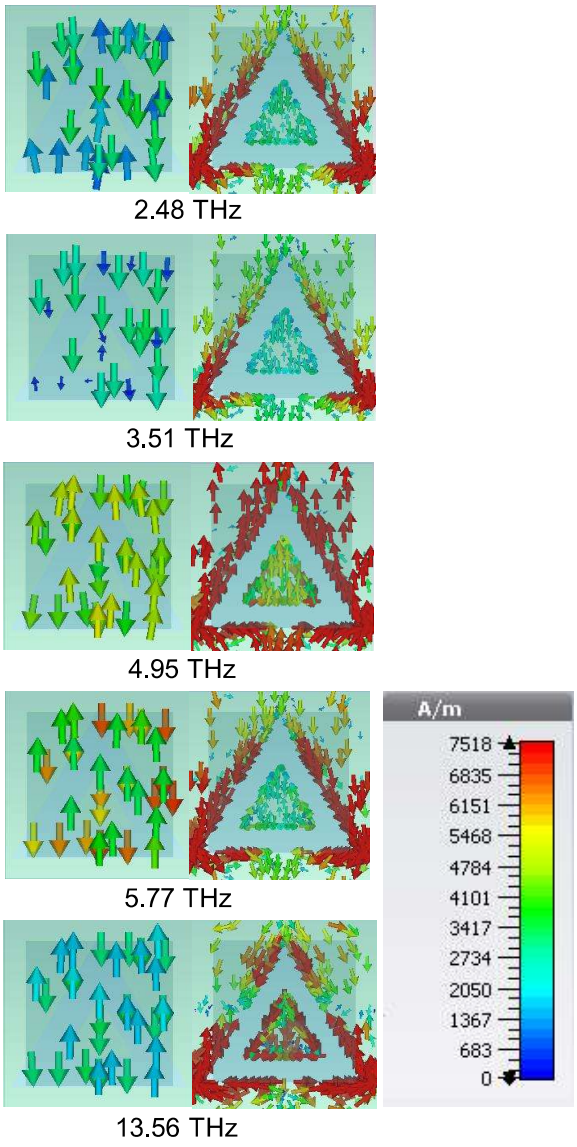

Fig. 3.20. Surface current distributions of the top layer and the bottom layer at different frequencies.

Further, the electric field distributions and current distributions of the structure are validated by the simulations at frequencies from 1 THz to 16 THz. The electric field distributions of the overall structure at different frequencies are provided in Fig. 3.19. The electric fields are dense at the vertical edges of the structure at 2.48 THz and 3.51 THz. The orientations of the electric field patterns at 4.95 THz and 5.77 THz are perpendicular to the previous one. A reduced centralized form of the previously discussed E-field patterns has been experienced at 13.56 THz from Fig. 3.19. The top layer and bottom layer orientations of the current vectors are

identical at 2.48 THz, 3.51 THz, and 4.95 THz, respectively. The orientations of the current vectors are opposite than the previous one, at 5.77 THz and 13.56 THz, respectively. The parallel orientation of the current vectors results in the electric excitation, while the anti-parallel orientation between them mimics magnetic excitation of resonance. It is clear from Fig. 3.20 that at 3.51 THz, electric excitation is dominant while at 5.77 THz, the magnetic excitation is dominant. The proposed rasorber design has been compared with rest of the existing literatures as given in Table 3.2. It can be found that the introduction of graphene on the top layer enables tunability of the performance by maintaining the compactness in design.

Further, it can be seen from Table 3.2 that the rasorbers in the gigahertz region provide larger fractional absorption bandwidth; however, their applications are limited due to incorporation of lumped elements in the metasurface designs [275]-[277]. The tunability has been reported in the graphene-based terahertz rasorber configurations [278]-[280]. It has been observed that the proposed rasorber configuration offers wide 10-dB fractional absorption bandwidth together with an enhanced 3-dB fractional transmission bandwidth and greater transmission coefficient maintaining the effective homogeneity condition as well as ultra-thin nature.

Table 3.2. Comparison with Existing Rasorber Structures

Rasorber Designs	**Structural Configuration**	**10-dB FABW**	**3-dB FTBW**	**PTC**	**FBO**	**Thickness**	**Periodicity**	**Angular Stability**
K. Zhang *et. al.* [266]	Metal-dielectric-metal	>80%	5%	0.955	2-10 GHz	~λ_g/2.73	~λ_g/1.68	Angular stability up to 60º
M. Guo *et. al.* [275]	Metal-dielectric-metal	>80%	12.2%	0.985	3-16 GHz	~λ_g/3.38	Non symmetric	Angular stability up to 30º
A. Li *et. al* [279]	Multilayer	93%	7.14%	0.977	5-35 GHz	~λ/2.94	~ λ_g	Angular stability not discussed
F. G. Meng *et. al.* [280]	Metal-dielectric-metal	64%	10%	0.822	2-18 GHz	~λ_g/5.47	~λ_g/3.32	Angular stability not discussed
X. Xiu *et. al.* [276]	Metal-dielectric-metal	114%	33.3%	0.971	1-7 GHz	~λ_g/4.99	~λ_g/2.08	Angular stability up to 30º
H. Huang *et. al.* [277]	Metal-dielectric-metal	112.4%	13%	0.967	1-11 GHz	~λ_g/2.22	~λ_g/1.20	Angular stability up to 20º
M. Qu *et. al*. [281]	Metal-graphene-dielectric-metal-graphene	>70%	2.58%	0.85	2.5-10 THz	~λ_g/4.61	~λ_g/2.22	Angular stability up to 40º for lower frequency band only
M. Qu *et. al*. [282]	Metal-graphene-dielectric-metal-graphene	100%	15.38%	0.825	0.2-1.2 THz	~λ_g/7.20	~λ_g/3.34	Angular stability up to 40º, not explicitly discussed
Q. Zhou *et. al.* [283]	Graphene-dielectric-metal	66.7%	12.12%	0.72	0.1-2 THz	~λ_g/2.70	~λ_g/1.87	Angular stability not discussed
This paper	Graphene-dielectric-metal	70.33%	34.01%	0.925	1-16 THz	~λ_g/10.70	~λ_g/12.49	Angular stability up to 60º

FABW: Fractional Absorption Bandwidth, # **FTBW**: Fractional Transmission Bandwidth, # **PTC**: Peak Transmission Coefficient # **FBO**: Frequency Band of Operation.

3.5. Conclusions

A graphene-based three-layered compact ($\lambda_g/12.49$) and ultrathin ($\lambda_g/10.70$) rasorber is discussed in this work. The device offers a tunable 10-dB fractional absorption bandwidth of 70.33% and a 3-dB fractional transmission bandwidth of 34.01% up to 40° incident angles of EM wave for both TE and TM polarizations. Tunability property of the absorption band without using any lumped component is an addition to this concept. The rasorber is polarization independent in the absorption band due to the four-fold symmetry of the top graphene pattern. The two-fold symmetry of the triangularly-slotted bottom surface enables slight shift of transmission band under oblique incidence. The proposed device can find efficient applications in several fields such as communication security, satellite-based communication systems, stealth applications, and several others.